

Supporting Information for the manuscript "The interfacial tension of nanoscopic oil droplets in water is hardly affected by SDS surfactant"

Hilton B. de Aguiar, Alex G. F. de Beer, Matthew L. Strader, and Sylvie Roke*

Max-Planck Institute for Metals Research, 70569 Stuttgart, Germany, Fax: +49-711-6893612

E-mail: roke@mf.mpg.de

This supporting information contains:

Supporting text regarding materials and methods, droplet stability, size distribution, creaming rates, Ostwald ripening, SFS spectra taken in multiple polarization combinations both for S-O and C-H stretching modes, the equation used in the modified Langmuir model, the effect of micelles, a change in surface tension calculated from SFG measurements on a planar interface, and a comparison between ζ -potential data and SFS scattering

Materials and Methods

Emulsions were prepared by mixing a 2 vol% mixture of n-hexadecane-d₃₄ (>98 %, Cambridge Isotopes) in D₂O solution (>99 %, Sigma-Aldrich) containing 100 μ mol purified SDS (>99 %, Alpha Aesar)¹ with an OMNI TIP homogenizer in a 5 ml vial. The resultant mixture was treated in an ultrasonic bath (35 kHz, 400 W Branson) for 15 minutes. This emulsion was used as a stock sample, which was further diluted with a solution of SDS in D₂O at a known concentration. In this way, emulsions with a constant volume fraction and droplet size were prepared with varying concentrations of SDS. The thus prepared emulsions were stable for months. The droplet size distribution was determined by dynamic light scattering measurements (DLS), using a Malvern ZS nanosizer.

ζ -potential measurements were done using laser Doppler velocimetry with the Malvern ZS nanosizer instrument, software package and disposable electrophoretic cell. On the electrodes of the cell an electric field is applied with both fast and slow components. Phase analysis light scattering is used to retrieve electrophoretic mobility that can be converted into a ζ -potential.²

The sum frequency scattering (SFS) measurements were done with the emulsions placed in a CaF₂ cuvette with an optical path length of 0.1 mm. The SFS experiments were performed using 10 μ J (150 fs) infrared (IR) pulses (repetition rate 1 kHz, FWHM bandwidth of \sim 140 cm⁻¹) centered around 1100 cm⁻¹ and 10 μ J, 800 nm visible (VIS) pulses with a 12 cm⁻¹ FWHM bandwidth (see Ref.³ for more details). The selectively polarized IR and VIS pulses were incident in the horizontal plane under a relative angle of 15° and focused down to a \sim 0.5 mm beam waist. The scattered light was measured in the same plane at a scattering angle of 60° around a solid angle of 20°. The SF photons were polarization selected and spectrally dispersed onto an intensified CCD camera (I-STAR, Andor Technologies). Fluctuations in laser power and stability were accounted for by measuring a reference sample between samples with different SDS concentrations.

¹The SDS was purified by multiple recrystallization cycles in water and ethanol until the surface tension on water at a total concentration of 4 mM SDS (measured with a Wilhelmy plate method) was no longer changing (see Ref.¹).

Droplet stability and size distribution

To determine the size distribution of the emulsions we performed DLS measurements on the droplets as a function of SDS concentration and as a function of time. Also, we calculated the creaming and Ostwald ripening rate for our water/hexadecane systems.

Fig S1A shows the average radius (blue squares, left axis) obtained for a concentration series that was used in the SFS experiments. The data points are averages of 5 measurements, and the error bars represent the width of the distribution. It can be seen that the droplet radius does not depend on the SDS concentration.

Fig S1B shows three size distribution measurements performed on the same sample (containing 8 mM SDS) with time intervals of a few hours, typical for the duration of a SFS measurement series. In the time span of our experiment, we were not able to measure a significant change in the droplet size distribution. The average droplet radius was 83 nm, with a standard deviation of 20 nm.

Fig. S1A shows ζ -potential data for the same emulsions for which the radius was determined. The values range from -74 to -116 mV and correspond to those of stable emulsions.⁴⁻⁶

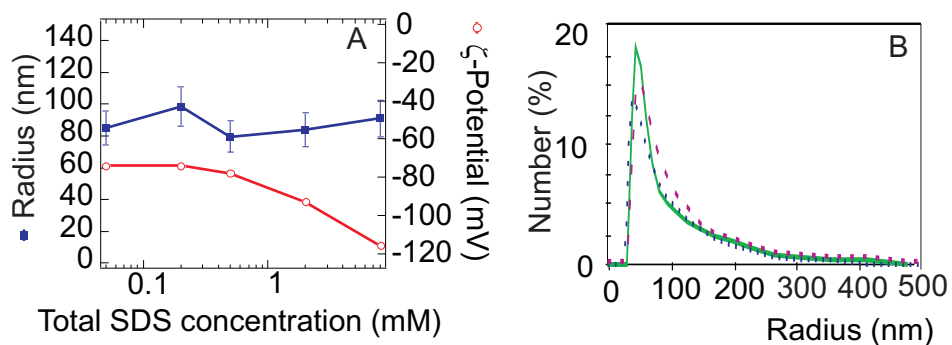


Fig. S1. Droplet stability and size distribution. Panel A: The left axis (blue squares) displays the average radius for droplets prepared with constant droplet size and varying concentration for a series of SFS measurements. The right axis (red circles) displays the ζ -potential for the same emulsions. Panel B: DLS measurements after preparation of an emulsion containing 8 mM SDS at time intervals of 0 hours (straight line), 3 hours (dashed line) and 6 hours (dotted line) after preparation.

Creaming, flocculation and Ostwald ripening

To further quantify the stability of our emulsions as a function of time we have calculated the creaming rate. The creaming rate (v) is given by the following expression:

$$v = (\rho_{C_{16}D_{34}} - \rho_{D_2O}) \frac{4R^2 g}{18\eta_{D_2O}} \quad (1)$$

where $\rho_{C_{16}D_{34}}$ is the density of deuterated hexadecane (796.3 kg/m³), ρ_{D_2O} is the density of deuterated water (1105 kg/m³), R is the average radius of the oil droplets, g is the local acceleration due to gravity (9.81 m²/s), and η_{D_2O} is the viscosity of deuterated water (1.25 mPa s).⁷ Inserting the given values we obtain a creaming rate of -3.44×10^{-9} m/s, which corresponds to a rise of 1.4 mm per week.

In order to measure the long-term size stability of the emulsions we have prepared a concentration series as described above, where we have used non-deuterated n-hexadecane (Sigma-Aldrich >99%) and Millipore water (18.2 M Ω cm). At various time interval a small volume from the prepared stock emulsions was diluted 100 times, after which the average droplet radius was measured. Fig. S2A shows radius data as a function of time for samples with varying SDS concentrations, over a time span of 10 days. The initial droplet size is a bit bigger, which occurs if we use non-deuterated hexadecane and water. It can be seen that the size increase is very slow. Since our SFS measurements were typically performed 3 hours after preparation we believe that the droplet sizes in a concentration series are constant and do not vary on the time scale of the measurement (typically not longer than 6 hours).

The Ostwald ripening rate can be calculated according to the Lifshitz-Slyozov-Wagner (LSW) model.^{8,9} The average radius as a function of time $\bar{R}(t)$ can be written as:

$$\bar{R}(t) = (\bar{R}(t=0)^3 + \frac{8\gamma D c_{r \rightarrow \infty} V_m^2 t}{9R_g T})^{1/3} \quad (2)$$

where γ is the interfacial tension at the oil-water interface, D is the diffusion coefficient of the oil

through the aqueous phase, $c_{r \rightarrow \infty}$ is the solubility of the oil in the aqueous phase, V_m is the molar volume of the oil, R_g is the gas constant and T is the absolute temperature.

The red curve in Fig S2B shows a calculation of the increase in droplet radius due to Ostwald ripening. For this calculation we have taken values for the solubility, the diffusion constant, the molar volume and the interfacial tension from Ref.⁹ It can be seen that indeed the Ostwald ripening rate for this system is very slow. It should be noted however that the measured Ostwald ripening rate presented in Ref.⁹ is much larger than what is calculated using Eq. 2. For an emulsion of 5wt % hexadecane oil in water with 20 mM SDS it was measured that the average radius increased from 51 nm to 63 nm in 480 hours (20 days). This data is represented in Fig. S2B by the dashed line. Although this rate is much higher than predicted by the calculation it is still very low. We would like to note that if we repeat the calculation with Eq. 2, with an interfacial tension value of 52 mN/m we arrive at an Ostwald ripening rate that is much closer to the measured value, as can be seen from the blue curve in Fig. S2B.

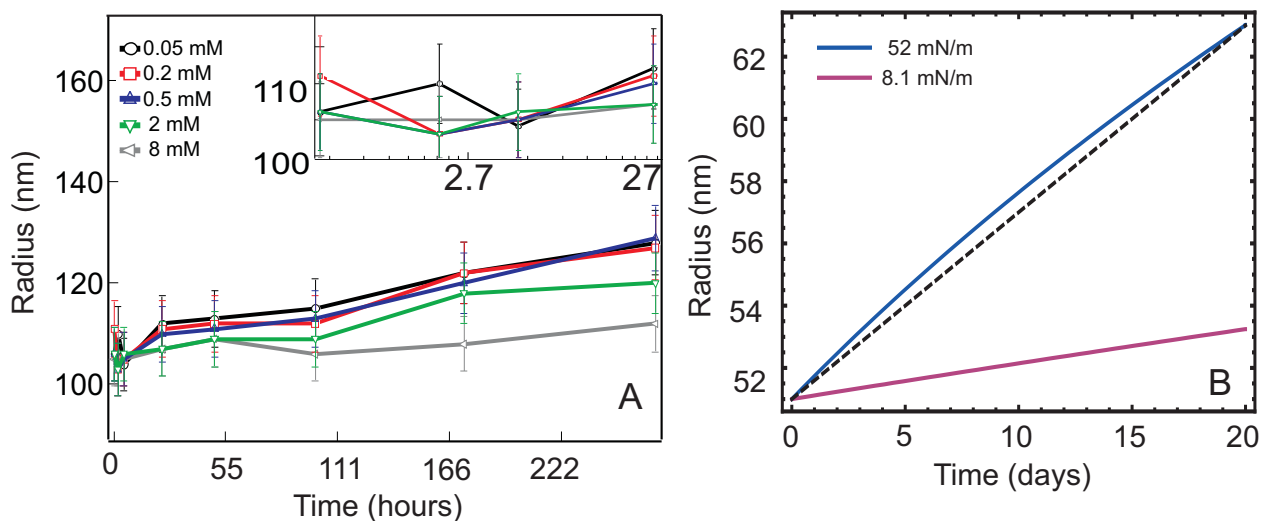


Fig. S2. A: Particle radius as a function of time (up to 10 days) for samples prepared with the method described above. The inset zooms in on the first 27 hours after preparation. B: The calculated Ostwald ripening rate using Eq. 2, using different values for the interfacial tension (γ). The dotted line corresponds to data points taken from Ref.⁹ (Figure 5).

SFS spectra in multiple polarizations and spectral regions

In order to convert the SFS data to a surface excess we need to assert that the molecular orientation (and conformation) is not changing as we change the total surfactant concentration. Also, we need to consider how the Fresnel factors are changing if we increase the concentration of SDS. Whether both effects have an influence on the measurements can be established by measuring SFS spectra for both the SO_3 and CH stretch mode in multiple polarization combinations. If both the *ssp* and *ppp* data for the SO_3 symmetric stretch mode display the same trend and if the conformation of the alkyl chains does not change, while the increase in overall signal in the CH stretching region displays an identical trend as the SO amplitudes we believe we can conclude that the SFS amplitude from the SO_3 symmetric stretch mode is linearly related to the increase in surface density.

SO_3 stretching mode region

Fig. S3 shows SFS spectra taken in the spectral region around the SO_3 stretch mode of SDS obtained for *ssp* and *ppp* polarization (for the other two allowed directions *sps* and *pss* the SFS signal was below our detection limit).

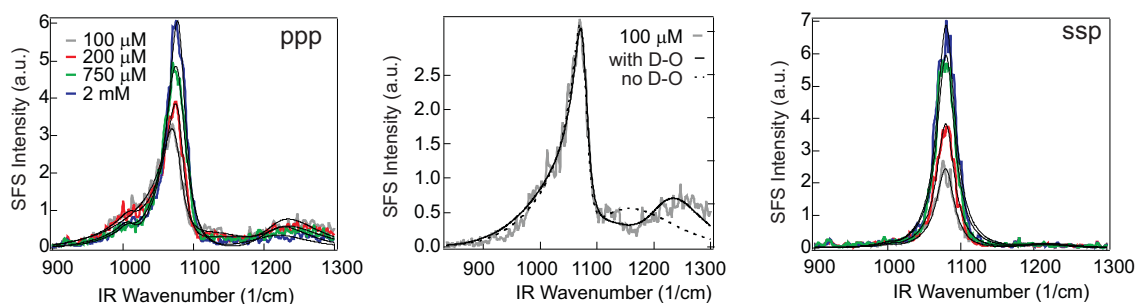


Fig. S3. Left panel: SFS spectra taken for emulsions with varying (total) concentration of SDS at a scattering angle (θ) of 60 degrees with polarization combination *ppp*. Middle panel: Spectra taken for an emulsion with a total SDS concentration of 100 μM , fitted with (black solid line) and without (black dashed line) taking into account the D-O bending vibration at 1215 cm^{-1} . Right panel: SFS spectra for the same samples in *ssp* polarization. The black lines are fits made with Eq. 3.

The SFS spectra were fit with the following equation:

$$I_{SFS}(\omega, \theta) \propto |\mathbf{E}_{IR}(\sum_n \frac{A(\theta)_n}{(\omega - \omega_{0n}) + i\Upsilon_{0n}} + A_{NR}e^{i\Delta\phi})|^2 \quad (3)$$

where n refers to a specific vibrational mode, with resonance frequency ω_{0n} , damping constant Υ_{0n} , and angle dependent amplitude A_n . E_{IR} is the envelope of the IR pulse and A_{NR} is the amplitude of the non-resonant contribution, which has a relative phase $\Delta\phi$.

The fits were made with the SO_3 symmetric stretch resonance at $\omega_{\text{SO}_3} = 1079.7 \text{ cm}^{-1}$, with a width of $\Upsilon_{\text{SO}_3} 15.0 \text{ cm}^{-1}$. As can be seen from the spectra, the *ppp* polarization is not only determined by this resonance but also by a 'non-resonant' background and a broad band around 1215 cm^{-1} , which coincides with the D-O bending mode of heavy water. The IR pulse was described by a fitted Gaussian centered around 1109 cm^{-1} with a width of 132 cm^{-1} . The visible pulse had a FWHM of 12 cm^{-1} .

Table 1: Fitting parameters for the spectra in Fig. S2

	<i>ppp</i>				<i>ssp</i>			
$c_{tot,SDS}$ (mM)	0.1	0.2	0.75	2	0.1	0.2	0.75	2
A_{SO_3}	1.18	1.49	2.21	2.80	1.60	2.02	2.53	2.80
A_{NR}	1.20	1.12	0.82	0.68	0.06	0.06	0.06	0.06
$\Delta\phi$	158	163	166	198	184	184	184	184

CH stretching mode region

Fig. S4 shows SFS spectra in the spectral region around the CH stretch mode of SDS obtained for *ssp* and *ppp* polarization. The baseline subtracted spectra were divided by the used power of the laser beams and acquisition time. Since all of the spectra for a single polarization have the same shape, they are related by a concentration-dependent scaling factor. The square root of this scaling factor is plotted for both *ssp* and *ppp* polarization and displays the same trend as the S-O data. Further, it can be seen very clearly that there is no change in average molecular conformation, since the spectral shapes for both *ssp* and *ppp* do not change.

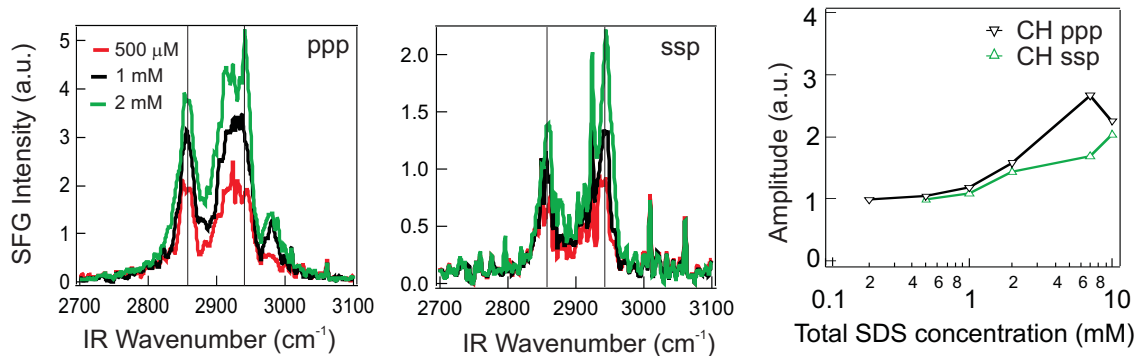


Fig. S4. Left panel: SFS spectra taken for emulsions with varying (total) concentration of SDS at a scattering angle (θ) of 60 degrees with polarization combination *ppp*. Middle panel: SFS spectra for the same samples in *ssp* polarization. The vertical lines are drawn at 2855 cm⁻¹, and at 2940 cm⁻¹. Right panel: The square root of the relative spectral intensities for different concentrations of SDS. The intensity for each polarization is set to 1 for the lowest concentration.

Scattering functions and the effect of micelles

Our analysis is based on the assumption that the SFS intensity relates linearly to the interfacial density of the droplets. This assumption could break down if the Fresnel factors of the interfacial layer change strongly as a function of total SDS concentration, or if micelles contribute to the signal. To consider both effects we need to know how the SFS intensity depends on the radius of the droplet or micelle.

The angle dependent amplitudes of the SFS field obtained for a polarization combination $u_0u_1u_2$ can be related to Eq. 3 by the following expression: $|A_n(\theta)|_{u_0u_1u_2}^2 = I_n(\theta)_{u_0u_1u_2}$. The electric field amplitudes can be found by applying the Rayleigh-Gans-Debye (RGD) approximation or exact Mie theory.¹⁰ The RGD approximation assumes that the difference in refractive index between the particle and the bulk medium is small enough so that the electric fields are not distorted when they move through the droplets. For the emulsions described in our manuscript we have a refractive index difference of ~ 0.1 and a radius of 83 nm, so that the criterium for the application of the RGD approximation ($\frac{2\pi}{\lambda} |(\frac{n_{water}}{n_{oil}} - 1)| < 0.1$) is satisfied. In order for it to deviate,

the refractive index of water at the interface would have to be smaller than that of the bulk, which is physically not realistic. Also, the effect of the addition of salt to water will have a very small effect on the refractive index. For example, when salt is added in a large amount (so that the weight percentage is 0.43 %, i.e. 74 mM NaCl), the refractive index of the solution changes from 1.33840 to 1.33920 for 632.8 nm light.¹¹ A similar effect can be expected for SDS. We therefore conclude it is safe to use the RGD approximation to model the data and predict the scattering pattern.

Using the following form factors:¹²

$$F_1 = 2iR^2 \left(\frac{\sin(qR)}{(qR)^2} - \frac{\cos(qR)}{(qR)} \right) \text{ and } F_2 = 4iR^2 \left(\frac{3\sin(qR)}{(qR)^4} - \frac{3\cos(qR)}{(qR)^3} - \frac{\sin(qR)}{(qR)^2} \right),$$

and abbreviated notations:

$$\chi_1 = \chi_{zzz}^{(2)} - \chi_{zxx}^{(2)} - \chi_{xzx}^{(2)} - \chi_{xxz}^{(2)}, \chi_2 = \chi_{xxz}^{(2)}, \chi_3 = \chi_{xzx}^{(2)}, \chi_4 = \chi_{zxx}^{(2)}, \text{ and}$$

$$\Gamma_1 = \Gamma_{zzz}^{(2)} - \Gamma_{zxx}^{(2)} - \Gamma_{xzx}^{(2)} - \Gamma_{xxz}^{(2)} = \pi\chi_1(2F_1 - 5F_2), \Gamma_2 = \Gamma_{xxz}^{(2)} = \pi(2F_1\chi_2 + F_2\chi_1), \Gamma_3 = \Gamma_{xzx}^{(2)} = \pi(2F_1\chi_3 + F_2\chi_1), \Gamma_4 = \Gamma_{zxx}^{(2)} = \pi(2F_1\chi_4 + F_2\chi_1),$$

the electric field components are given by:

$$E_{ppp} \propto \Gamma_1 \cos\left(\frac{\theta}{2}\right) \cos\left(\frac{\theta}{2} - \alpha + \beta\right) \cos\left(\frac{\theta}{2} - \alpha\right) + \Gamma_4 \cos(\beta) \cos\left(\frac{\theta}{2}\right) + \Gamma_3 \cos(\theta - \alpha) \cos\left(\frac{\theta}{2} - \alpha + \beta\right) + \Gamma_2 \cos(\theta - \alpha + \beta) \cos\left(\frac{\theta}{2} - \alpha\right) \quad (4)$$

$$E_{ssp} \propto \Gamma_2 \cos\left(\frac{\theta}{2} - \alpha\right) \quad (5)$$

$$E_{sps} \propto \Gamma_3 \cos\left(\frac{\theta}{2} - \alpha + \beta\right) \quad (6)$$

$$E_{pss} \propto \Gamma_4 \cos\left(\frac{\theta}{2}\right) \quad (7)$$

were $\chi_{ijk}^{(2)}$ are the elements of the second-order nonlinear susceptibility, β is the angle between the IR and VIS beams, and α is the angle between the forward direction (i.e. the sum of the IR and VIS wave vectors) and the IR wave vector. θ is the scattering angle, which is defined as the angle of the scattered light (with wave vector \mathbf{k}_0) with respect to the forward direction. q is the scattering wave number:

$$q = 2|\mathbf{k}_0| \sin(\theta/2) \quad (8)$$

To estimate the contribution of micelles to the scattering signal we have calculated the scattered intensity of both a micelle and an emulsion droplet. The result is shown in Fig. S5.

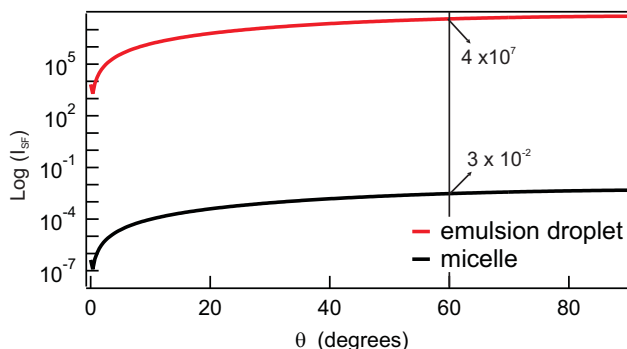


Fig. S5. Calculated sum frequency scattering intensity as a function of scattering angle for an emulsion droplet ($R=80$ nm, red curve) and a micelle ($R=2$ nm, black curve). The intensity was calculated for polarization combination ssp , using the parameters of the experiment. The graphs are plotted on a log scale. It can be seen that the signal of an emulsion droplet measured at $\theta=60^\circ$ (indicated by the vertical line) is 9 orders of magnitude larger than that of a micelle.

It can be seen that in our experiment a single micelle scatters 9 orders of magnitude less than an emulsion droplet. Since we perform our SFS measurements below the c.m.c., it is unlikely that there are many micelles present. Nevertheless, if we assume that at 8 mM all SDS is in the form of a micelle we have (per ml of solution) 4.8×10^{16} micelles and 4.6×10^{12} emulsion droplets. Because the total scattered intensity increases linearly with the number of droplets or micelles the total difference in scattering intensity between droplets and micelles amounts to a factor of $\frac{4.8 \times 10^{16}}{4.6 \times 10^{12}} 10^{-9} \approx 10^{-5}$. Thus, we can neglect any contribution of scattering from micelles to our signal. To corroborate the result we have performed scattering experiments on solutions of 30 and 60 mM SDS in water, and were not able to detect any scattered sum frequency light.

Retrieval of surface excess from amplitude data

The strength of the second-order nonlinear susceptibility is directly proportional to the molecular hyperpolarizability $\beta^{(2)}$ and the density of molecules N_s (in mol/m²) at an interface, according to:

$$\chi_{ijk}^{(2)} = N_s N_{avo} \langle T_{ia} T_{jb} T_{ck} \rangle \beta_{abc}^{(2)} \quad (9)$$

where $\langle T_{ia} T_{jb} T_{ck} \rangle$ is the average result of the coordinate transformation from a molecular frame of reference $((a, b, c))$ to the coordinate frame of the interface $((i, j, k))$ and N_{avo} is Avogadro's number ($N_{avo} = 6.022 \cdot 10^{23}$). $\chi^{(2)}$ determines the strength of the nonlinear scattering amplitude according to eqns 4-8. The scattering form factors F_1 and F_2 as well as the parameters θ and α do not change during the experiment. The measured signal amplitudes are therefore directly proportional to $\chi^{(2)}$ and thus to the density of molecules at the interface: $E_{SFS} \propto N_s$. In order to get a physically realistic estimate of the surface excess, the number of absorbed molecules ($N_s A$, with A the total area of the oil-water interface in the sample) may never exceed the overall number of molecules present ($c_{tot,SDS} V$, with V the total sample volume) in a sample. The entire N_s vs c curve must therefore lie below the line $N_s = c_{tot,SDS} V / A$. Because it is unlikely that all SDS molecules reside at the interface (while none remain in the water phase), we have estimated the surface coverage by fitting the data in Fig. 1C with the modified Langmuir model presented by Wang et al. in Ref:¹³

$$E_{SFS} \propto \frac{N_s}{N_s^{max}} = \frac{c_s}{c_s^{max}} = \frac{(c_{tot,SDS} + c_s^{max} + c^\ominus / K) - \sqrt{(c_{tot,SDS} + c_s^{max} + c^\ominus / K)^2 - 4c_{tot,SDS} c_s^{max}}}{2c_s^{max}} \quad (10)$$

whereby we have imposed the condition that

$$c_{tot,SDS} V \geq N_s A \quad (11)$$

where c_s is the concentration of absorbed molecules (so that $c_{tot,SDS} = c + c_s$), T is the temperature, c^\ominus is the molarity of water and K is a constant that can be related to the free energy of adsorption

(ΔG) by $\Delta G = -R_g T \ln K$, with R_g is molar gas constant. The maximum droplet surface coverage N_s^{max} and the Gibbs free energy of adsorption ΔG are the fitting parameters. The fit presented in Fig. 2A was made with parameters: $3.92 \pm 0.13 \times 10^{-7}$ mol/m² for the saturation surface coverage (N_s^{max}), and -29.10 ± 0.58 kJ/mol (ΔG). Although the quality of the fit is not excellent it does provide an upper limit for the surface excess. It should be noted that fits with the same accuracy could also be reached with smaller values of N_s^{max} .

Extracting the surface tension from SFG data: the planar SDS/air/water system

We have verified that the interfacial tension and molecular surface density obtained from SFG measurements can be related to each other by analyzing SFG data obtained from SDS adsorption on a planar air/water interface.¹⁴

Fig. S6 shows surface tension measurements for the air/water interface as a function of SDS concentration (red circles, left y-axis),¹⁵ The blue line plotted on the right axis represents the change in surface tension as obtained from the SFG intensity data plotted in Ref.¹⁴ Here, we used the known surface density of SDS at the c.m.c., as a reference point.

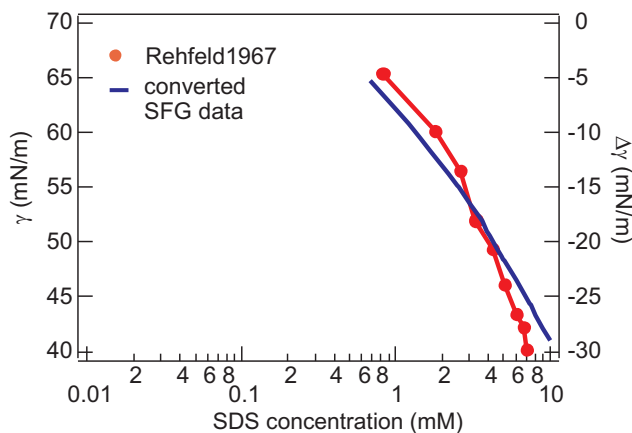


Fig. S6. Surface tension data for the SDS/air/water system (left axis), in combination with the retrieved change in surface tension by using the Gibbs equation and the SFG data from Ref.¹⁴

Correspondence between SFS and ζ -potential data

The surface charge density (σ) can be retrieved from calculating the electrokinetic charge present at the shear plane. Assuming that this plane is very close to the particle interface, the surface charge density can be retrieved using the following approximation:²

$$\sigma = \varepsilon_0 D \frac{kT}{ze} \kappa \left(2 \sinh(z\zeta/4) + \frac{4}{\kappa R} \tanh(z\zeta/4) \right) \quad (12)$$

with ε_0 the permittivity of free space, D the relative permittivity ($D = \frac{\varepsilon}{\varepsilon_0}$), κ the Debye-Hückel parameter $\kappa = \sqrt{\frac{e^2 \sum_i n_i^0 z_i^2}{D \varepsilon_0 k T}}$, k the Boltzmann constant, T the temperature, e the elementary charge, z the valency, and n_i^0 the number of ions of type i in de bulk solution.

Although it is not certain that all the SDS is ionized at the interface, it is clear that the value found for the charge density and the value found for the surface excess from the SFS experiments should be of the same order of magnitude. As is shown in Fig. 2A, they are.

References

- (1) Lunkenheimer, K.; Pergande, H.-J.; Krueger, H. *Rev. Sci. Instrum.* **1987**, *58*, 2313–2318.
- (2) Hunter, R. J. *Zeta potential in colloid science*; Academic Press, 1981.
- (3) Sugiharto, A. B.; Johnson, C. M.; de Aguiar, H. B.; Aloatti, L.; Roke, S. *Appl. Phys. B.* **2008**, *91*, 315–318.
- (4) Hunter, R. J. *Foundations of Colloid Science*; 2002.
- (5) Marinova, K. G.; Alargova, R. G.; Denkov, N. D.; Velev, O. D.; Petsev, D. N.; Ivanov, I. B.; Borwankar, R. P. *Langmuir* **1996**, *12*, 2045–2051.
- (6) Beattie, J. K.; Djerdjev, A. M. *Angew. Chem. Int. Ed.* **2004**, *43*, 3568 – 3571.
- (7) Vanysek, P. *Handbook of Chemistry and Physics*; CRC Press, 1995.

- (8) Lifshitz, I. M.; Slyozov, V. *J. Phys. Chem. Solids* **1961**, *19*, 35–50.
- (9) Weiss, J.; Herrmann, N.; McClements, D. J. *Langmuir* **1999**, *15*, 6652–6657.
- (10) de Beer, A. G. F.; Roke, S. *Phys. Rev. B* **2009**, *79*, 155420–1–9.
- (11) Lu, W.; Worek, W. M. *Appl. Opt.* **1993**, *32*, 3992 – 4002.
- (12) Roke, S. *Chem. Phys. Chem.* **2009**, *10*, 1380–1388.
- (13) Wang, H. F.; Yan, E. C. Y.; Liu, Y.; Eissenthal, K. B. *J. Phys. Chem. B* **1998**, *102*, 4446–4450.
- (14) Johnson, C. M.; Tyrode, E. *Phys. Chem. Chem. Phys.* **2005**, *7*, 2635–2641.
- (15) Rehfeld, S. *J. Phys. Chem.* **1967**, *71*, 738– 745.